Gating the Conductivity of Arrays of Metallic Quantum Dots

F. Remacle,[‡,†,⊥] K. C. Beverly,[||] J. R. Heath,[||] and R. D. Levine*[,†,§]

The Fritz Haber Research Center for Molecular Dynamics, The Hebrew University of Jerusalem, Jerusalem 91904, Israel, Département de Chimie, B6c, Université de Liège, B4000 Liège, Belgium, Department of Chemistry and Biochemistry, University of California, Los Angeles, Los Angeles, California 90095, The Division of Chemistry and Chemical Engineering, California Institute of Technology, MC 127-72, Pasadena, California 91125

Received: August 8, 2003; In Final Form: October 1, 2003

Experimental and computational studies demonstrating that the conduction of compressed, two-dimensional arrays of hexagonally ordered Ag quantum dots (QDs) may be varied through the influence of applied electric fields are reported and discussed. Monolayers of Ag QDs are incorporated into three-terminal (gated) devices, in which temperature, source-drain voltage (V_{sd}), gating voltage (V_g), compression of the array, and QD size distribution may all be varied. Experimental and computational results are compared in an effort to construct a physical picture of the system. Current vs V_{sd} plots at low temperatures exhibit systematic nonlinearities that change over to an ohmic-like behavior at higher temperatures and/or higher V_{sd}. The voltage-induced transition is discussed as a transition of the conducting states from domain localized to delocalized. Such a transition was previously observed in the temperature dependence of the resistance. The computational model reveals that this transition is also highly sensitive to both the compression of the array and the size-distribution of the dots. We calculate the influence of V_g on the conductivity of the QD array, using the same computational model. In both the experiment and the model, we find a significant voltage gating effect and we observe hole-type conductivity of the array. Overall, the results demonstrate that low-temperature transport measurements provide a spectroscopic-like probe of the electronic states of the QD lattice. The theoretical approach further suggests that quite different gating behavior can be observed for electrodes with a different Fermi energy than the gold electrodes used in the experiment.

I. Introduction

Designing materials, devices, and even systems of devices at the nm length scale is a rapidly evolving field. Its realization in the laboratory depends on a large number of new technologies including materials synthesis,[1,2] spectroscopic imaging techniques that provide chemical and structural information at the nm scale,[3] and the controlled assembly of the component building blocks into larger scale structures that can be probed and manipulated.[4] In this paper we discuss two-dimensional (2D) lattices assembled from organically passivated metal quantum dots (QDs). The emergent properties (see ref 5 and references therein) of such systems were first studied and understood at the level of the individual dots themselves.[6,7] Subsequent attention has been directed toward understanding unique properties of assemblies of interacting QDs. For example, these highly controllable systems may serve as models for understanding electronic transport in reduced dimensions.[8−13] As we present here, the outlines of a broad understanding of these systems are beginning to emerge. We make this point by demonstrating the close agreement between theory and experiment in interpreting the conductance spectra of voltage-gated 2D arrays.

Small metallic QDs are, in many ways, uniquely suited models for understanding transport in reduced dimensions, because several experimental advantages combine to make the theoretical picture simple. First, narrow size distribution samples of organically passivated metallic QDs can be readily prepared and assembled into well-ordered hexagonally packed monolayers,[14−16] with defect free domain sizes extended from hundreds to thousands of dots. The size of a dot determines the energies of the higher (valence) electronic orbitals. Therefore, the array is not only geometrically ordered but it is also almost electronically ordered. Consider a single-particle thick hexagonal domain containing a few thousand particles. If the dots are separated by a distance (D) that is <20% of the diameter ($=2R$) of the metallic cores (i.e., $D/2R < 1.2$), then the wave functions of the valence electrons overlap significantly and the dots are exchange coupled. Because of the narrow size distribution, adjacent dots are almost resonantly coupled. Acting against charge transfer from one dot to another is the Coulomb blocking potential, or charging energy. Put simply, this is the finite energy cost of adding an electron to a dot that already has its share of electrons. For QDs only a few nm in diameter, the charging energy, while small compared to the charging energy of a single atom, is finite and typically larger than k_BT at room temperature. Taking account of the charging energy is technically not easy because it is a correlation between different electrons, and so requires moving beyond a single electron approximation. Including the role of the Coulomb repulsion results in a separation between the covalent and the ionic states.[17] The gap between these states will be closed when the charging energy is smaller than the exchange coupling between adjacent dots. This is the well-known Mott transition[18] from an insulator to a

* Corresponding author. E-mail: rafi@fh.huji.ac.il, fax 972-2-6513742.
† The Hebrew University of Jerusalem.
‡ Université de Liège.
§ University of California.
|| California Institute of Technology.
⊥ Maître de Recherches, FNRS, Belgium.

10.1021/jp036357h CCC: $25.00
Published on Web 11/18/2003

metal. For the array, such a transition can be readily induced (and observed) by reducing $D/2R$ (via compression) so that the coupling (exponentially) increases. Computational results[17,19] clearly show the closing of the gap between the covalent and ionic bands.

For QD arrays there is, however, another mechanism whereby ionic and covalent states can exist in the same energy range. This has to do with the finite dispersion in sizes of the dots. For an array of identical dots, the ionic states are at higher energy because of the finite charging energy. Thus, a state ..DDD$^+$D$^-$DD.. is higher in energy than the state ..DDDDDD... However, for low-charging energies and nonidentical QDs, this is not necessarily so. The reason is that the size determines the ionization potential (IP) of a dot. If one dot has a lower than average IP and its neighbor has a higher than average IP, the difference $\Delta\alpha$ of the IPs may be sufficient to more than compensate for the charging energy, and the band of ionic states will merge with the band of covalent states. Because the states of different character are nearly resonant, even a weak exchange coupling can lead to state mixing. We have previously investigated both small (3 nm)[20] and large (7 nm)[21,22] diameter QDs. Here we discuss primarily the larger QDs that have a relatively low charging energy ($\sim$0.1 eV). For these systems, a one electron molecular orbital approximation, where ionic and covalent states are mixed, provides a sufficiently realistic description, particularly at low values of $D/2R$.

We have previously argued that domains of nanodots can exhibit electronic polymorphism[19] and have compared the experimental static measurements of the surface potential as a function of voltage, degree of disorder, and compression with the theoretical predications.[23,24] This comparison[23] provided the direct demonstration that the effect of the V_{sd} is not simply that of a weak external probe. The system cannot be simply described as responding linearly to the voltage. Rather, there are qualitative changes in the states of the array depending on the external voltage. What that proof lacked was the ability to probe a limited range of states within the system. In this paper we provide that demonstration and specifically report that nonlinearities in current vs voltage plots[25] are seen experimentally. We further show that these nonlinearities are typical of a low temperature, low V_{sd} regime and that increasing either one of these control parameters induces a transition to an activated conduction regime where the response is much more linear.[21] As a validation of this picture we gate the source-drain conductivity through the application of an additional gating voltage (V_g) applied perpendicular to the array. Here, too, we report a close agreement between experiment and theory.

An implication of our conclusion is that measurements of the conductance do not necessarily provide the spectroscopy of the isolated array. Because of the high density of states and of the low size disorder that is required for the current to be measurable, it is only at rather low voltages and low temperatures that what is being probed by the conductance is the density of states of the domain itself. Otherwise, the states of the array significantly respond to the external voltage and what we are probing is the density of states of the device. We consider that this is good rather than bad news. An I vs V_{sd} curve teaches us not only about the unperturbed array (from the behavior near the origin) but also on how we can modify the states of the array by the application of the voltage (or by changing the Fermi level of the electrodes). In some sense what we are observing is the Stark spectra of the dense set of electronic states. Like the Stark spectra of high Rydberg states[26,27] that are also very dense in energy, there is new physics that can be gleaned. To avoid misunderstanding we mention already here that, because of the high density of electronic states, the onset of nonlinear behavior can be at quite low V_{sd}. Experiment and theory concur that this occurs at a voltage gradient of about 2×10^{-4} volts per dot.[28]

The theoretical formalism that allows us to naturally treat the nonlinearities is realized by including the role of the external voltage in the zero-order Hamiltonian description of the array. This makes the states of the array voltage dependent. Otherwise we use a standard scattering-theory approach,[29] which, in appearance, is similar to the Landauer formalism.[30−35] The differences are in the details. In section II we provide the essential points that are relevant to the discussion here and also emphasize the many-electron description that we use, a description that highlights the difference between electron and hole conduction. We refer to a complete presentation of the formalism elsewhere.[36] One simplification here is that we shall treat only elastic charge migration. That is, we will not allow the electron (or hole) to heat or cool the array. This is not an essential limitation but it makes for a more tractable computational problem for a reason discussed in more detail in section II. In essence, the point is that we are interested in the effect of temperature. This requires a two-fold sum. One sum is over the thermally accessible states of the electrodes and a second sum over the thermally accessible states of the array. There are very many (N electron) electronic states of the array. So this second sum, while trivial, is computationally tedious. If we allow inelastic processes, we need yet another sum over the array, where this is a sum over all accessible final states of the array because these need not be the same as the initial states.

Section III compares experimental and computational results for current vs voltage at different temperatures. It serves to validate the model Hamiltonian and the computational method used. It concludes that a quantum phase transition can be seen experimentally both by varying the temperature and, even more dramatically, by varying the V_{sd}. In section IV another control variable is brought to bear, V_g. The agreement between experimental and computational results provides, for us, the critical validation of our interpretation. With this comparison we believe that we have achieved our stated goal. Beyond it, we have shown how gating experiments provide a valuable and critical extension of the spectroscopic probing that can be achieved by transport measurements. This is because it is possible to use a low V_{sd}, so that the array is unperturbed and the Fermi (observation) window is quite narrow, and to tune the range of states that are being probed.

II. Theoretical Considerations

The Hamiltonian we use has been extensively compared, see ref 13 for a perspective, to experimental probes of the static and dynamic electronic responses of arrays of quantum dots. The Hamiltonian contains several parameters, and these have the same values as in our earlier work.[37] It is a one-electron tight binding (or Hückel) Hamiltonian that neglects the role of charging energy blocking. This means that the covalent (with one electron at most per site) and ionic states (where at least one site is doubly occupied) are fully mixed and, as we have extensively discussed,[37,38] this is realistic for compressed arrays but will fail otherwise.

The degree of compression is usually reported as the value of $D/2R$, where D is the distance between the centers of adjacent dots and $2R$ is the (mean) diameter of a dot. The exchange

coupling was parametrized by the following analytical form:

$$\beta = (\beta_0/2)(1 + \tanh((D_0 - D)/4RL)) \xrightarrow{D>2R} \beta_0 \exp(D_0/2RL) \exp(-D/2RL) \quad (1)$$

The coupling strength saturates to its maximum value β_0 when the dots are nearly touching one another and decays exponentially at large interdot separation. The parameters of the functional form (1) were determined by fitting the experimental nonlinear SHG response for 3.5-nm diameter Ag QDs and were used unchanged in all subsequent computations.[37,39] The strength of the exchange coupling, β, between adjacent dots scales as $\exp(-\kappa D)$ where the screening length, $\kappa = 1/2RL$, is typical of the chemical nature of the dot. In the effective mass model, it corresponds to the length scale of the leaking out of the radial Bessel function outside of the QD. We have checked that both estimates are in agreement.[40] The term $1/\kappa$ is expected to be independent of the size of the dot. This implies that, for larger dots, $1/2L$ has to be larger. The fall off curve of the exchange coupling vs $D/2R$ for the 7 nm QDs used in the latest experimental measurements of the conductivity is plotted in the left upper panel of Figure 1. The upper panel on the right is the corresponding curve for smaller dots with a diameter of 3.5 nm. The value of the compression at the onset of strong coupling, $D_0/2R$, depends on the diameter of the dots and for large dots occurs at smaller values of $D_0/2R$. The size-dependence of D_0 can be expressed as $D_0 = 2R + d_0$, where d_0 is size independent. When plotted vs $D - 2R - d_0$, β has a universal character for all the sizes. For 7 nm dots, strictly strong coupling requires $D/2R < 1.25$. The experiments and computations that we report are at $D/2R \cong 1.22$ and below.

Figure 1 shows that smaller dots are significantly coupled over a wider range of compressions (measured in terms of $D/2R$).[37] However, they have a larger charging energy ($I \propto 1/R$) so that the Coulombic effects cannot be neglected, except at higher compressions when the metallic cores of the QDs are almost touching one another. At intermediate compressions, the covalent and ionic bands are not merged. This can be seen from the lower panels in Figure 1 that show the transition frequencies, ω_{ng}, between the ground and the excited many-electron states of a 7×7 electron array, as a function of $D/2R$ for 3.5 nm and 7 nm dots, both with 5% disorder in sizes and 5% packing disorder. These computations use a Hubbard Hamiltonian, which takes into account the on-site Coulombic repulsion. The right lower panel is computed for 3.5 nm dots for which $I > \Delta\alpha$ and therefore, at large interdot separation, the covalent states are by I lower in energy than the ionic states. The relevant parameter for the merging of the ionic and covalent bands is that $(6\beta)^2/I$ be of the order of I. In that case, the ground state is ionic.[17] On the other hand, when $\Delta\alpha > I$ (7 nm dots, lower left panel), the bands of ionic and covalent states are also merged at large values of $D/2R$. The reason is that the fluctuation in site energies is wider than the charging energy, so that an ionic state where low energy sites are doubly occupied can be lower in energy than a covalent state. This implies that when $\Delta\alpha > I$, the Hückel description is useful over a wider compression range. Of course, for a sufficiently expanded lattice the exchange coupling becomes too weak and the ionic and covalent states will not be effectively mixed.

The elements of the tight binding Hamiltonian matrix for the array itself are

$$H_{ij}^0 = \begin{cases} \alpha_i \text{ for the diagonal elements} \\ \beta_{ij} \neq 0 \text{ for near neighbors only} \end{cases} \quad (2)$$

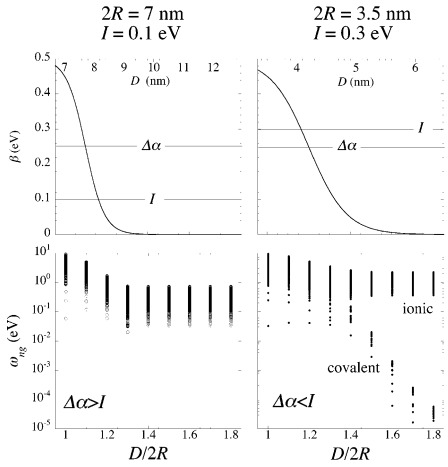

Figure 1. Falloff curves (eq 1) for the exchange coupling β and the corresponding transition frequencies in eV vs $D/2R$ (lower scale) and D (upper scale) for Ag QDs 7 nm in diameter (left panels) and 3.5 nm in diameter (right panels). For both sizes, the universal parameters are $\beta_0 = 0.5$ eV, $\kappa = 3.143$ nm^{-1} and $d_0 = 0.7$ nm. For 3.5 nm dots $1/2L = 5.5$ and $D_0/2R = 1.2$, while for 7 nm dots $1/2L = 11$ and $D_0/2R = 1.1$. Also shown as a straight line is the value of the charging energy, I, for the two sizes ($I = 0.3$ eV for 3.5 nm dots and 0.1 eV for 7 nm dots). As discussed in the text, I is to be compared not only to 6β but also to the range, $\Delta\alpha$, of orbital energies due to size variations and, for a given disorder, $\Delta\alpha$ has the same value for dots of either size. (The factor 6 is the number of neighboring dots.) Smaller dots are exchange coupled over a wider range of compression than larger dots, but the Coulombic effects cannot be neglected until the onset of very strong coupling. In this study, we report computational and experimental results for dots 7 nm in diameter, where the neglect of Coulombic effects in the strong exchange coupling regime is realistic, for size variations of over about 3%. The computation of the transition frequencies includes 5% fluctuation in size and 5% packing disorder. They are carried out using a Hubbard Hamiltonian for a 7-site, 7-electron array. For 3.5 nm dots (right panel), $\Delta\alpha > I$. At large interdot separations, the Coulomb energy is the strongest perturbation, leading to a band of covalent states and higher by I, bands of ionic states. The covalent states are not exactly degenerate because they are coupled by the exchange coupling in second and higher orders. The two bands merge (in the, so-called, Mott transition) when the exchange coupling is strong enough to bridge for the Coulombic effects. Full delocalization occurs when the dots are nearly touching one another so that β also fully bridge the differences in site energies due to fluctuation in sizes. (This is the Anderson transition.) The bottom panel on the left is for 7 nm dots, so that $\Delta\alpha < I$. Now the ionic states are not confined to higher energies because $\delta\alpha_i$ in eq 3 can be larger than I. Covalent and ionic states can be almost degenerate and such states are effectively mixed by the exchange coupling. As discussed in the text, such coupling is still local in character and it requires strong exchange coupling to produce globally delocalized states. The resulting transition is discussed in section III.

Here α_i is the energy of the highermost (singly) occupied orbital of the ith dot

$$\alpha_i = \alpha_0 + \alpha_0\delta\alpha_i + eV_g + eV_i \quad (3)$$

and contains four terms. Here, e is the electron charge, $\alpha_0(1 + \delta\alpha_i)$ is the orbital energy of the ith dot in the absence of any voltage where α_0 is the mean energy, and $\alpha_0\delta\alpha_i$ is the change from the mean due to variation in sizes. In other applications the first term, namely the value of α_0 itself, is immaterial as it only sets the zero of energy. Not so in the presence of the electrodes. The difference between α_0 and the Fermi energy of the electrode is a critical variable, and we return to this point below. The effect of the gate, not introduced until section IV, is the third term. V_g is applied in a direction normal to the array, see Figure 2, but it is shielded by a dielectric layer so that the

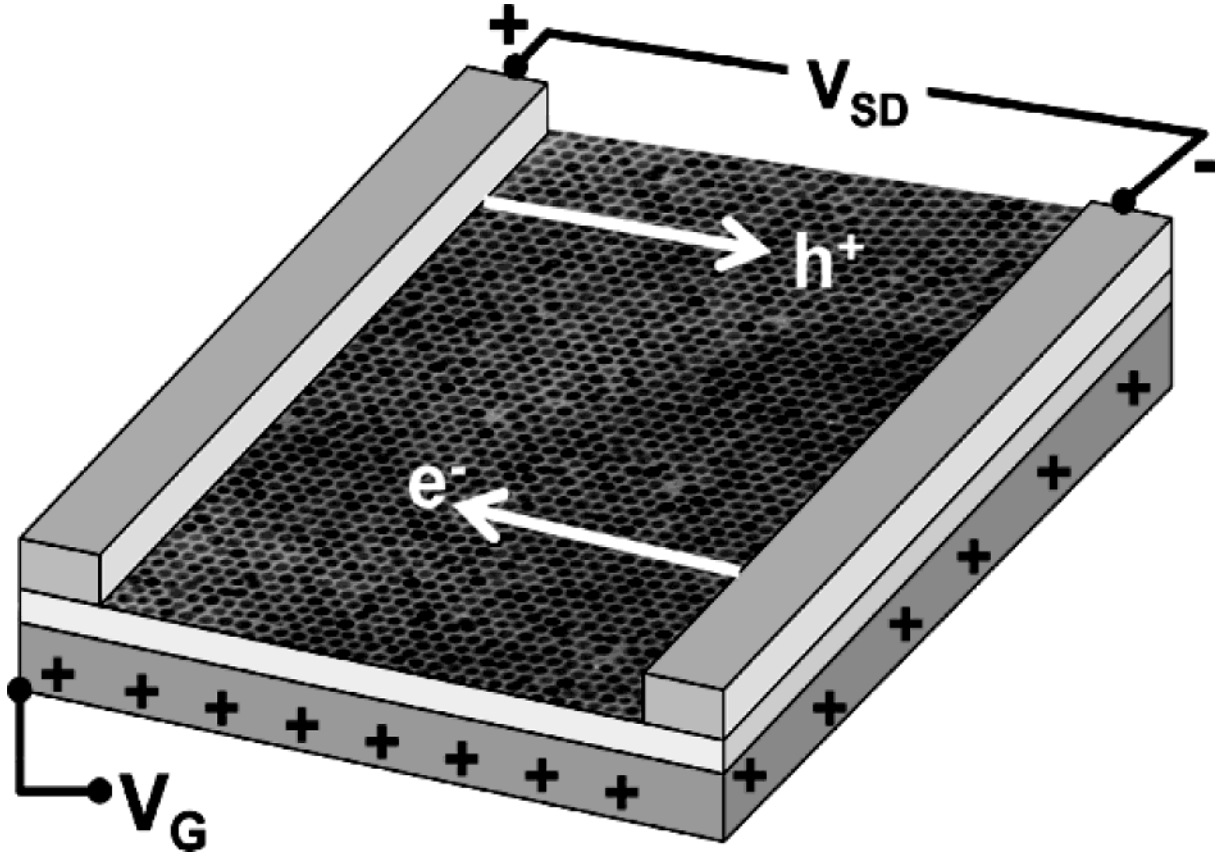

Figure 2. Schematic view of the geometry of the device, showing both the QD monolayer, the source and drain contacts, and the gate electrode. Charge transport within such arrays was investigated experimentally as in previous work (refs 21, 22). The 7-nm diameter Ag nanoparticles with a finite but small size distribution of 7% were transferred in a fashion similar to ref 21 from the air−water interface of a Langmuir trough onto heavily doped Si wafer coated with 100 nm SiO_2 and patterned with gold electrodes. The incorporation of a gate electrode is novel and is accomplished by the back gating of the silicon substrate on which a 100 nm thick thermally grown silicon oxide dielectric layer is grown and subsequently patterned with source drain electrodes. Gating voltages of up to ±70 V were applied to the Si wafer. The field at the device is mitigated by the spanning dielectric SiO_2, and so the field experienced by the QD array is very much smaller than the applied bias. Both possible mechanisms for conduction (electrons into conduction band states and holes into valence band states) are depicted.

V_g that we use is significantly smaller than the nominal value. Equation 3 does not account for the shielding of V_g by the electrodes. This shielding is expected to reduce the effect of the gate only for those dots near to either electrode, see Figure 2. The Stark shift of the orbital energy due to the V_{sd} is accounted for by the last term.[41] We take the voltage gradient to be linear so that V_i is determined by the distance of the ith dot from the electrodes.

The array we use is hexagonal with 55 dots per side so that there are 8911 dots and the matrix $\mathbf{H}^0$ is 8911 by 8911. This matrix is diagonalized in order to determine the one-electron states of the array. By analogy to molecules, we can refer to them as the orbitals of the array. In addition to the energies of these states, what plays a crucial role is the weight of these orbital states on the dots that are adjacent to the electrodes. We will quantify this statement later, but as a simple guide, only those orbitals of the array that have a nonnegligible weight on the dots that are near the electrode on the right *and* on the dots that are near the electrode on the left will contribute to the conductivity. Much of the localization effects that we will discuss are due to this simple condition.

In addition to the Hamiltonian of the array, the zeroth order description includes the one-electron states of the two electrodes. We take these to be states of a free electron gas, with a Fermi energy at E_F and designate these states by i and f for the left and the right electrodes, respectively. In the presence of an applied V_{sd}, there is a Stark shift of these free electron energies so that the two Fermi energies are shifted up and down respectively by $eV_{sd}/2$. The current is driven by a coupling, U, between the electrodes and the array. We take U to be a one-electron transfer operator of localized range so that only those dots in direct contact with the electrodes are coupled to them.[42] U can either move an electron from the electrode to the array or move a hole in the other direction. Schematically we can write for electron conduction

$$\mathrm{LAR} \xrightarrow{U_L} \mathrm{L^+A^-R} \xrightarrow{U_R} \mathrm{L^+AR^-} \tag{4}$$

and for hole conduction

$$\mathrm{LAR} \xrightarrow{U_R} \mathrm{LA^+R^-} \xrightarrow{U_L} \mathrm{L^+AR^-} \tag{5}$$

where we put a subscript on U to distinguish the couplings on the two sides. In the experimental setup the coupling to the two electrodes is of equal strength, but this need not be so in general. The two mechanisms are the reason we use many-electron states to describe the array. In the case of electron conduction, the intermediate state of the array has $N + 1$ electrons, while for hole conduction it has $N - 1$ electrons.

The initial and final states of the complete system (array and the two electrodes) are $N + 1$ electron states of the full zero order Hamiltonian. Since the coupling U between the electrodes and the array is not included in the zero order description, the zero order states are products of a state of the array and of the states of the two electrodes. In the initial state, the array is neutral and is described by an N electron state built as an anti-

symmetrized product of the one-electron orbitals of the array, $|\Phi_N\rangle^N = \Pi(\phi_\mu)^{f_\mu}$, where f_μ is the occupation number (0 or 1) of the orbital ϕ_μ. In $|\Phi_N\rangle^N$, the subscript N means the array has N sites while the superscript N means it has N electrons. The left electrode is occupied by one electron and the right electrode is empty:

$$|I\rangle = |i\rangle^1 \, |\Phi_N\rangle^N \, |f\rangle^0 \tag{6}$$

For elastic transmission, the state of the array is the same in the final state but an electron has migrated from the left to the right electrode:

$$|F\rangle = |i\rangle^0 \, |\Phi_N\rangle^N \, |f\rangle^1 \tag{7}$$

In the case of electron conduction, the intermediate state, L^+A^-R in eq 4, has $N + 1$ electrons on the array and no electron on the electrodes: $|i\rangle^0 \, |\Phi_N\rangle^{N+1} \, |f\rangle^0$, while for hole conduction, the intermediate state, LA^+R^- in eq 5, has $N - 1$ electrons on the array and one electron on each electrode. It is written as $|i\rangle^1 \, |\Phi_N\rangle^{N-1} \, |f\rangle^1$. Note that the description of the intermediate state in terms of separable zero order states is only valid in the limit of weak coupling to the electrodes.

In the scattering approach that we use,[36] the current, I, is proportional to the stationary rate of change of the charge on the right electrode, $\mathrm{d}\langle P\rangle/\mathrm{d}t$:

$$I = 2e\frac{\mathrm{d}\langle P\rangle}{\mathrm{d}t} \tag{8}$$

where using the generalized Ehrenfest theorem, for a 2D array, the stationary rate of change is given by

$$\frac{\mathrm{d}\langle P\rangle}{\mathrm{d}t} = \frac{2\pi}{\hbar}\sum_{I,F}(P_\mathrm{F} - P_\mathrm{I})\,\langle F|T(E)|I\rangle\delta(E_\mathrm{I} - E_\mathrm{F})\langle I|T(E)|F\rangle \tag{9}$$

$T(E)$ is the transition operator, $T(E) = U + UG(E)U$. In the limit of weak coupling to the electrodes, $G(E) \equiv (E - H^0 - U)^{-1}$ is replaced by the Green's function of the uncoupled system $G^0(E) \equiv (E - H^0)^{-1}$, but the effects of V_sd and of V_g are included in H^0. P_I and P_F are the thermal weights of the initial and final states (eqs 6 and 7). Each of them is a double sum over the one-electron states of the electrode, weighted by a Fermi function and over the thermally accessible N electron states of the array, weighted by a Boltzmann factor. $\langle F|T(E)|I\rangle\delta(E_I - E_F)\langle I|T(E)|F\rangle$ is the transmission function of the array.

In the weak coupling limit, the amplitude $\langle I|T(E)|F\rangle$ is a sum over the orbitals of the array:

$$T_\mathrm{IF}(E) = \langle I|T(E)|F\rangle = \sum_\lambda T_\mathrm{IF}(\lambda) \tag{10}$$

with, for a given orbital ϕ_λ,

$$T_\mathrm{IF}(\lambda) \approx i\pi U^2\sum_k\sum_{k'} c_{k\lambda}\delta(E - E_\lambda)c_{k'\lambda} \tag{11}$$

where $c_{k\lambda}$ and $c_{k'\lambda}$ are the amplitudes of the orbital ϕ_λ on the sites k and k' that are directly coupled by U to the electrodes. Equation 11 shows why, for an orbital of the array to conduct, it needs to have significant weights on sites that are coupled to the left and to the right electrode. $T_\mathrm{IF}(E)$ is therefore a weighted density of conducting states.

The transmission function of the orbitals of the array varies widely from one orbital to the next (Figure 3). It depends on the strength of the exchange coupling, β, on the amount of disorder in the site energies, $\Delta\alpha$, and on the strength of the source-drain bias, V_sd. The Figure 3 panels are computed for an array of 8911 dots with packing and size disorder and V_sd as indicated. The width of the band of conducting states is roughly proportional to 6β. This is because not all the QDs in the array have the same connectivity (the middle QDs have 6 near neighbors, while the dots on the edges have a connectivity of 3) and not all the QDs have the same effective coupling, $6\beta/\Delta\alpha$, because of the fluctuation in the sizes and of the packing disorder. When $\beta \ll \Delta\alpha$ (Figure 3B), the width of the band of conducting states is given by the range of the fluctuation in the site energies, $\Delta\alpha$. The width of the band of conducting states is also affected by the strength of the source-drain bias. At high source-drain bias strengths (when $eV_\mathrm{sd} > \Delta\alpha$, Figure 3D), the band of conducting states is narrower than at low values of V_sd (Figure 3A−C). The reason is that when the V_sd is the dominant perturbation, the amplitudes $c_{k\lambda}$ and $c_{k'\lambda}$ (eq 11) of highest or lowest energy orbitals (at the edges of the band) cannot be simultaneously large on both sides of the array.[25] The band is then narrower at both ends.

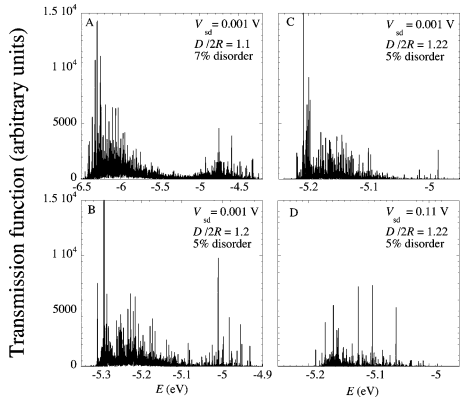

Figure 3. Transmission functions plotted versus energy and computed for a hexagonal array of 8911 dots, 55 dots per side. A disorder value of, for example, 7% correlates to both 7% in packing disorder as well as a 7% size distribution. (A) Computed for a highly compressed array. For this high coupling, the band of conducting states extends over a wide range in energy and exhibits a gap around the HOMO. (B) At lower values of $\beta/\Delta\alpha$ the band of conducting states is narrower and the gap is more filled by disordered states. (C) Here $\beta \ll \Delta\alpha$, and in this weak coupling situation the width of the band is controlled by $\Delta\alpha$. Note that the disorder is the same as in B. This array therefore exhibits the highest energy at which transmission starts. Increasing the coupling will allow transmission at lower energies. The states above the HOMO have a significantly lower transmission. (D) Transmission function vs energy computed at a high source-drain bias. Note that the spectrum of conducting states is much narrower at high bias strengths.

In the absence of disorder, $T_\mathrm{IF}(E)$ exhibits a gap around the highest occupied orbital.[37] For strengths of the effective exchange coupling $6\beta/\Delta\alpha$ that are high enough, the gap is still present (Figure 3A). However, as the ratio $6\beta/\Delta\alpha$ decreases, the gap around the highest occupied molecular orbital, HOMO, is filled by disorder and the overall intensity decreases since the orbitals of the array become more and more localized. The transmission function is not symmetric around the HOMO, and the decrease of intensity is more pronounced for the orbitals above the HOMO.

As can be seen from Figure 3, the low lying excited states around the HOMO are less conducting than excited states higher in energy. Computations[43] and static surface potential (SP) imaging[23] have shown that, for these states, the charge is delocalized over a finite but restricted number of states. We call this phase a domain-localized phase and it is a distinct phase

between the insulating phase at large interdot separation and the metallic phase typical of high compression levels.[12,19]

The domain-localized states are very sensitive to the effect of an external bias. The effect of V_{sd} is to induce correlation between the site energies in the direction parallel to it, while the site energies remain uncorrelated in the other directions. At intermediate compressions, moderate bias strengths, for which the Stark shifts, eV_{sd}, are comparable to the difference in energies due to the size disorder, $\delta\alpha_i$, result in a stripe structure in the SP images,[23] where the stripes are oriented parallel to the direction of the voltage gradient. In the absence of an external field, the islands are randomly oriented. The elongated shape of the islands in the presence of a field comes from the fact that the Stark shifts assist or disfavor charge delocalization in the direction parallel to the voltage gradient by compensating or increasing the energy mismatch between the sites, while there is no such effect in the other directions. When a moderate V_{sd} is applied, the domain-localized states thus lead to islands of higher charge, elongated along the direction of the voltage gradient. At higher V_{sd}, the array becomes Ohmic-like with contours of isocharge perpendicular to the voltage gradient.

In the domain localized regime, conduction is via variable range hopping (VRH)[18,44] made possible by a superexchange mechanism:[45] the coupling can be more efficient between two dots that are not adjacent but whose energies are almost degenerate. In this regime, conduction occurs via electron hops between the islands of higher charge. Note that here, the energy differences between the sites are due to the disorder in sizes and not to Coulombic effects, as is typically the case for semiconductors.[46] Higher excited states are less sensitive to disorder effects, are more delocalized, and have a higher transmission function. As discussed in section III, the temperature dependence of the current is different for the two kinds of states. It follows an $\exp(-(T_{VRH}/T)^{1/2})$ VRH law in the domain-localized regime and switches to an activated $\exp(-T_{act}/T)$ behavior in the activated regime.[21,37]

The final working expression for the current is obtained by using eqs 11 and 10 in eq 9 and taking care of the delta functions.[36] For a 2D array, it is a double sum over the thermally accessible N electron states of the array, $|\Phi_N\rangle$, in the initial state, and over the orbitals of the array ϕ_λ:

$$I = \frac{4\pi^3 e}{h}\sum_{\Phi_N} \exp(-E_{\Phi_N}/kT)\sum_{\lambda} g(\epsilon_\lambda,V,T)\,|T_{IF}(\lambda)|^2 \quad (12)$$

The double averaging leads to a Bolztmann weight $\exp(-E_{\Phi N}/kT)$for the states of the array. Because of the delta function in eq 11, the Fermi window $g(E,V,T)$ is computed at the energy ϵ_λ of the orbital ϕ_λ. The Fermi window is given by the difference between the Fermi functions of the left and of the right electrode:

$$g(E,V,T) = f_f\left(E - E_F + \frac{eV_{sd}}{2}\right) - f_i\left(E - E_F - \frac{eV_{sd}}{2}\right) = \frac{\sinh \upsilon}{\cosh \upsilon + \cosh x} \quad (13)$$

where $x = (E - E_F)/kT$ and $\upsilon = eV_{sd}/2kT$. At low temperatures and low V_{sd}, eq 13 looks like a delta function over E. However, due to the high density of low lying excited states that is typical of QD arrays, even at low bias and low temperatures, there is a finite number of states that fall within the Fermi window. This point is illustrated in Figure 4, where Fermi windows computed at a fixed low bias strength ($V_{sd} = 0.0022$ V) but for increasing temperatures (10, 100, and 300 K) are plotted for a

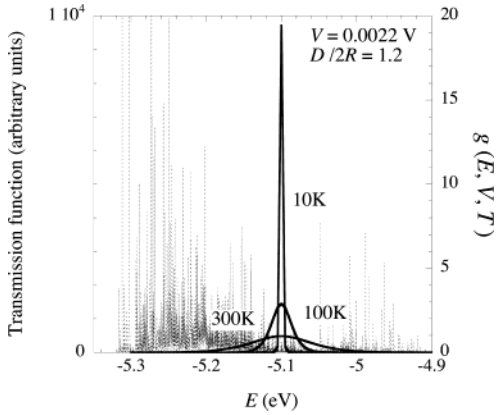

Figure 4. Fermi windows (eq 12) plotted for a low source drain bias ($V_{sd} = 0.0022$ V) but at three different temperatures. Shown in the background is the transmission function for an array with 5% disorder in sizes and in packing, computed at a level compression $D/2R = 1.2$ for the same value of V_{sd}. The Fermi level of the electrode is at -5.1 eV and falls close to the HOMO so that at low temperatures conduction is via domain localized states. At higher values of T, the better delocalized states are reached. As is shown by this figure, shifting the levels of the array with respect to the Fermi level of the electrodes by applying a gate voltage (or by changing the compression, see Figure 3) can drastically change the conductance.

Fermi level energy, E_F, equal to -5.1 eV. Also shown is the transmission function computed at the same V_{sd} strength for an array with 5% disorder in sizes and in packing at a compression level $D/2R = 1.2$. As the width of the Fermi window increases, more and more states contribute to the current. These states, however, do not have necessarily the same conducting character. The low lying excited states around the HOMO are domain-localized states while states higher in energy are more delocalized. This change in the conduction properties of the excited states with energy is the cause for the voltage-induced transition discussed in section III and for the exponential increase of the current with increasing temperature. The effect of V_g can also be understood from Figure 4. Changing the position of the Fermi level of the electrodes with respect to the band of conducting states will lead to different current curves. If E_F falls in the range of the domain-localized states, increasing V_{sd} or the temperature leads to a switching from a VRH mechanism to an activated one. If E_F is lowered to the bottom of the band by the application of V_g, only activated states will contribute to the current. This shows that varying V_g in a systematic way can provide spectroscopic information about the conducting states, as discussed in section IV below.

III. Conductance and the Voltage-Induced Transition

Experimental $I-V$ curves for an array of 7 nm diameter Ag dots with 7% disorder in sizes at a compression level $D/2R = 1.1$ are plotted in Figure 5A for increasing temperatures. At low temperatures, the $I-V$ curves have a sigmoid shape and are nonlinear with respect to the source-drain bias. They clearly exhibit two slopes: a low slope at low V_{sd} values and a larger slope at higher V_{sd}. As the temperature increases, the break occurs for smaller values of V_{sd}. When the temperature is sufficiently high (>30 K for the dots of the sample shown in Figure 5A), the current becomes linear with respect to V_{sd} and the behavior of the array is Ohmic. This is the experimental signature of the voltage-induced transition that was previously predicted theoretically.[38] It is clearly present in the computed $I-V$ curves, shown in Figure 5B for the same parameters of the array. The corresponding transmission function for these

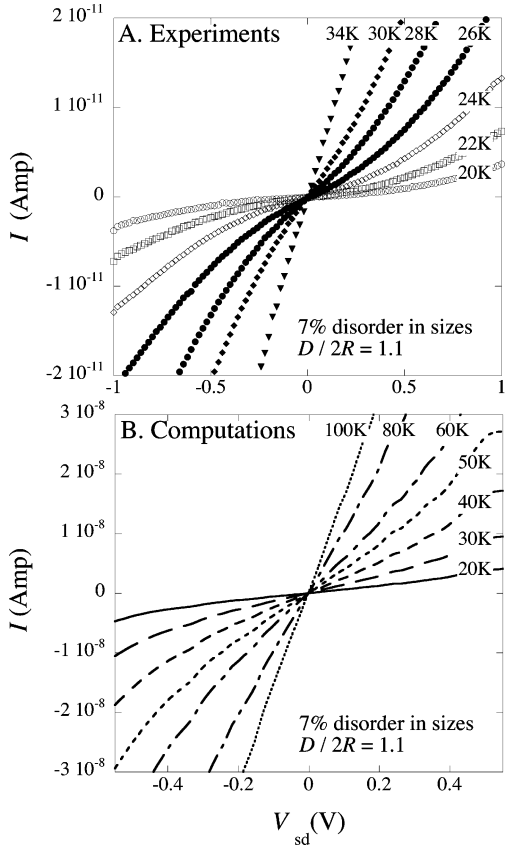

Figure 5. Experimental and computed $I-V$ curves. (A) The experimentally measured $I-V$ curves from an array of 7 nm Ag nanoparticles with a 7% size distribution and $D/2R = 1.1$. (B) The calculated $I-V$ curves computed for an array of 8911 dots with 7% fluctuation in size and 7% packing disorder. $2R = 7$ nm and the compression level, $D/2R = 1.1$. The experimental details are as in refs 21 and 22.

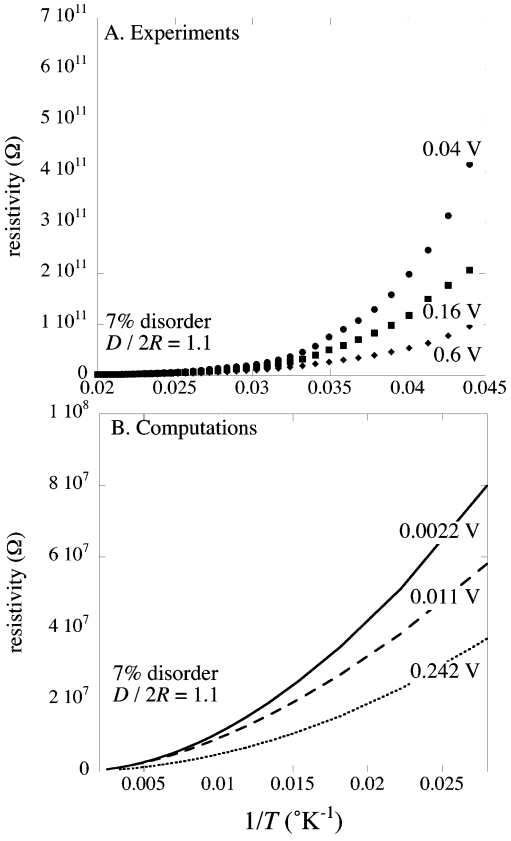

Figure 6. Experimental and computed resistivity vs $1/T$. The resistance for the experimentally measured films (top) is extracted from the measured $I-V$ traces (Figure 5A) by fitting the slope of the $I-V$ trace at each temperature point. The calculated resistivity (bottom) values from the array presented in Figure 5B were obtained as the inverse of the differential conductance, dI/dV, which is computed analytically.

parameters is plotted in Figure 3A. The generic behavior is identical, with a nonlinear, two slope behavior of the current curve at low temperatures that switches to a linear, Ohmic-like behavior at higher temperatures.

In the computations, the temperature range over which the transition takes place is larger than in the experiments. This is because the computations are for an array of approximately 1 μm in diameter, while the size of the ordered domain in the experiments is from 5 to 10 μm, which corresponds to about 25 to 100 times more dots and an accordingly higher density of states. From Figure 4 it is clear that what matters is how many orbitals of the array fall within the Fermi window whose width, at low V_{sd}, is kT. Therefore the dimensionless temperature should go as ρkT, where ρ is the density of orbitals. At higher voltages, that is, in the Ohmic regime, eq 13 shows that experiment and computations can be compared at the same temperature.

Any comparison between experiments and computations should also note that current is defined as the rate of charge transfer. It is clearly verified by the computations that each dot that is in contact with the electrode contributes about the same to the total current. Therefore, the larger the contact area with the electrodes, the higher the computed current.

A third factor important for the comparison between computed and measured currents is the strength of the coupling to the electrodes, U, which enters in the expression of the current (eqs 12 and 11) to the fourth power. We used in the computational results reported here a weak array−electrode coupling that is 10 times smaller than the exchange coupling inside the array. But because the experimental results shown in Figure 5 are for a very compressed array, $D/2R = 1.1$, the exchange coupling and hence U are high. We should not scale U down to fit the experiment because, as discussed above, the measured current should be about 5−10 times higher than the computed one because of the number of dots in contact with the electrodes. Another reason for care in scaling the computations to fit the experiment is the exponential dependence of the experimental results on the amount of size disorder (Figure 3 in ref 21) and compression. If we increase the size distribution by even 1% or decrease $D/2R$ by 1−2%, see Figure 8 below, we will decrease the computed current by an order of magnitude. This remarkable sensitivity is a manifestation of the underlying quantum phase transition, as we discuss next.

The low-temperature transition in the slopes of $I-V$ curves plotted in Figure 5 is a manifestation of the switching of the mechanism for conduction from a VRH behavior at low temperature to an activated behavior at high temperature.[37] It is also clearly exhibited when the differential conductivity, dI/dV, or the resistivity is plotted as a function of temperature, as in Figure 6. Here the experimental and computed resistivities for the same array as Figure 5 are plotted as $1/T$. As in Figure 5, the temperature range over which the transition takes place is smaller in the experiments (Figure 6A) than in the computation. Note that the absolute strengths for V_{sd} are smaller in the computations than in the experiments. This is again due to the smaller QD array size used in the model. The computations are carried out for the same voltage drop per dot as in the experiment. As the strength of V_{sd} increases, there is a switching to purely activated, $\exp(T_{act}/T)$ behavior while the two regimes

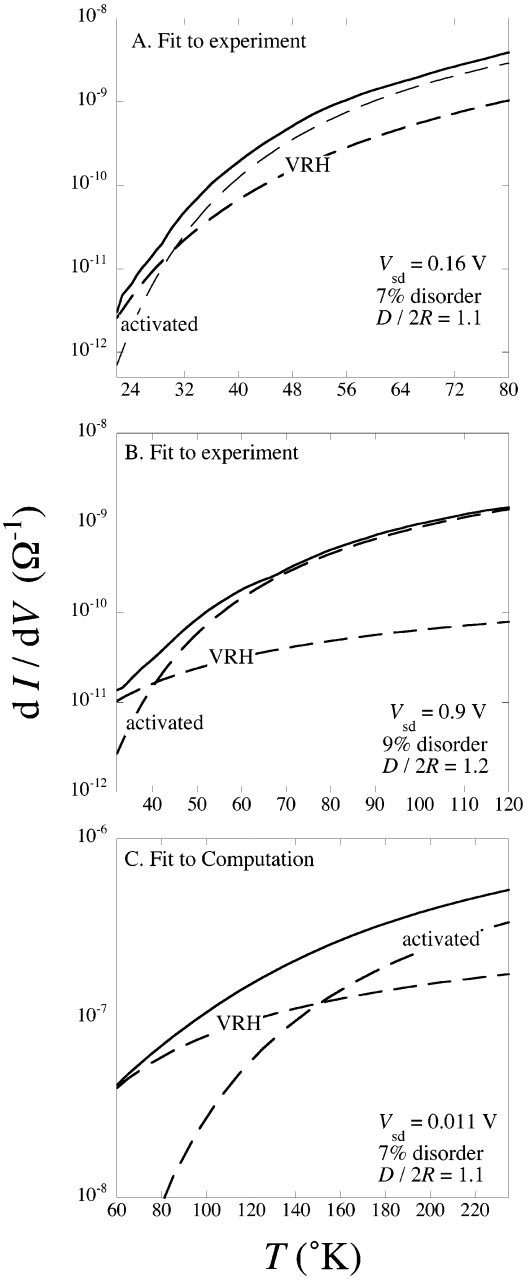

Figure 7. Resolution of the experimental (A and B) and calculated (C) dI/dV for 7 nm dots into two components. The fit is to dI/dV = A exp$(-(T_{VRH}/T)^{1/2})$ + B exp$(-T_{act}/T)$. (A) An array with 7% disorder at $D/2R$ = 1.1. T_{VRH} = 349.4 K, T_{act} = 258 K, and T_{cross} = 30 K. (B) An array with 9.2% disorder at $D/2R$ = 1.2. T_{VRH} = 561.4 K, T_{act} = 273.3 K, and T_{cross} = 41 K. (C) Computational results from an array with the same parameters as were used in the plots of Figures 5B and 6B.

(VRH in exp$(T_{VRH}/T)^{1/2}$ and exp(T_{act}/T)) coexist for lower V_{sd} strengths. At high temperatures, all the curves coalesce and exhibit activated behavior. The switching between the two components is shown in Figure 7A,B where the experimental differential conductivity, dI/dV, is plotted on a log scale with respect to the temperature for two different arrays. In the top panel, the compression is high enough that the VRH mechanism, assisted by V_{sd}, coexists with the activated regime at high temperature. The more disordered array requires a higher V_{sd} to induce the transition to activated conduction, but the VRH is disfavored, so the transition is sharper. For a given amount of disorder and compression level, as the strength of V_{sd} increases, the temperature (T_{cross}) at which the two components cross increases because the effect of V_{sd} is to assist conduction

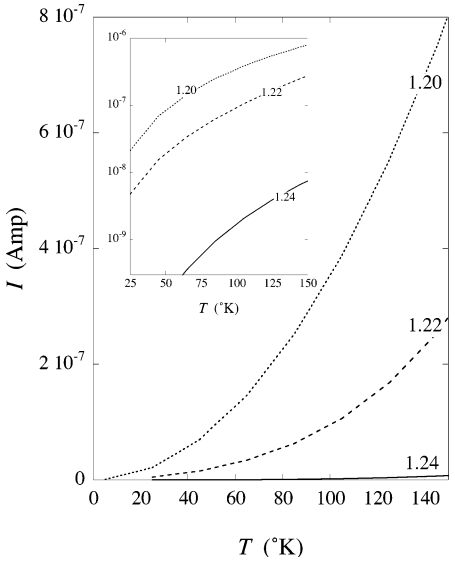

Figure 8. Metal, domain-localized and insulator conduction vs temperature. The change is brought about by a change in the compression. The current is computed for an array with 5% fluctuation in size and 5% packing disorder at the compression levels indicated. 2R = 7 nm. The value of the current saturates at about $D/2R$ = 1.21. Below $D/2R$ = 1.26 the current is too low to be measured. The inset shows the same data on a logarithmic scale.

in the VRH regime. The same trends are present in the computational results, as shown in Figure 7C for an array of 7 nm dots with 7% disorder in sizes and 7% packing defects at a level compression $D/2R$ = 1.1. The switching occurs at higher temperature than in experiments, due to the smaller density of states (smaller array size).

To conclude this section, we show the effect of compression on the current vs T curves. The computations are for an array with 5% fluctuation in size and 5% packing disorder at V_{sd} = 0.0088 V. There is a significant drop in the value of the current between $D/2R$ = 1.21 and 1.22, reflecting the metal-to-domain localized transition. For $D/2R$ > 1.23, the current is negligible and the array behaves as an insulator. The inset in Figure 8 shows the behavior of the current on a log scale.

IV. The Gate

Gating experiments can significantly extend the scope of transport measurements. The resolution in such experiments is governed by the width of the Fermi window. The width is narrower at lower temperatures and at lower V_{sd} (eq 13). Additional states can be brought into the window only by increasing the temperature and/or the applied bias. But then, as we have seen in section III, we need to unravel the contribution from states of different character. What the gating experiments and the companion computations show is that there are two ways of changing the energy of the few states that are probed by a narrow Fermi window. In either way, what we want to do is to change the relative value of the Fermi energy of the electrodes and the energy of the band of conducting states.

One way is to change the electrodes, although this can also modify the coupling to the array. As the computational results will show, there can be dramatic effects due to relatively modest changes in the Fermi energy of the electrodes, and so such a change is worthwhile.

The second way is to apply a gate voltage to the entire array and thereby manipulate the position of the energy levels of the array with respect to the Fermi energy of the electrodes. When a V_g is applied, conduction may not occur through the same

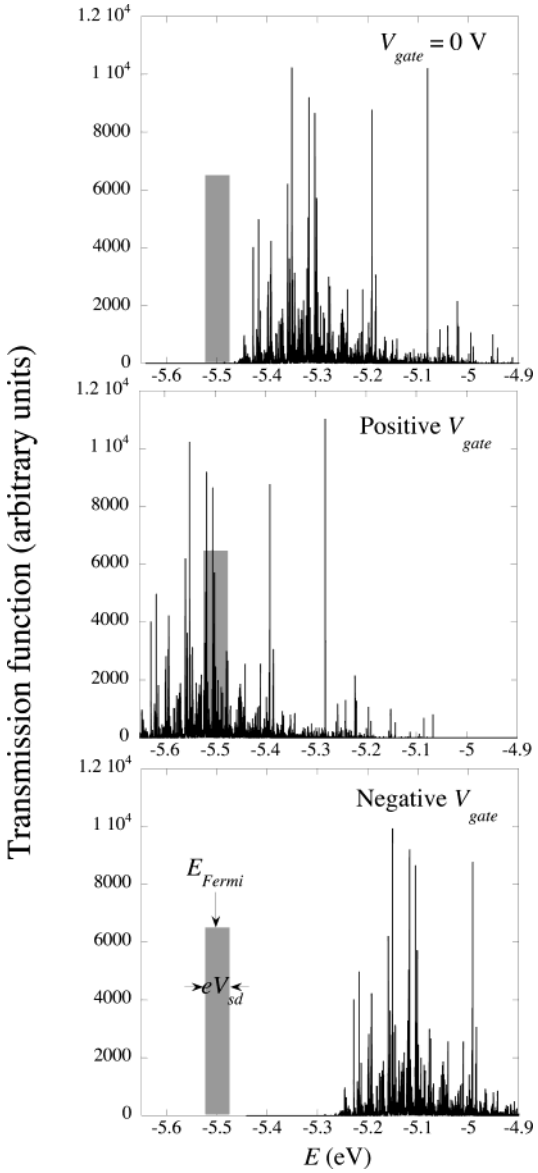

Figure 9. Effect of a gate voltage on the transmission function computed at $D/2R = 1.18$ for an array with 8% fluctuation in site energies and 8% packing disorder for a source-drain bias of 0.022 V. The top panel is computed in the absence of a gate voltage. Indicated is the position of the Fermi level of the electrodes ($E_F = -5.5$ eV) and the width of the Fermi window, shown shaded, at low temperature. In the middle panel, a positive gate voltage, whose effect is to move down the levels of the array by 0.2 eV, has been applied. States with a higher transmission function and a better conducting character now fall within the Fermi window and are responsible for the measured current. When a negative gate voltage is applied (bottom panel) so that the levels of the array are moved up by 0.2 eV, there are no significantly conducting states in the Fermi window and the current cannot be measured.

electronic states as in its absence, and this results in a change in the $I-V$ curves. By systematically varying V_g one can sweep the entire band of conducting states. For example, Figure 9 reveals the transmission function, the position of the Fermi level of the electrodes and, about it, a Fermi window (shaded). Figure 9A shows the transmission function at $V_g = 0$, computed for an array with 8% fluctuation in size and 8% packing disorder at compression level $D/2R = 1.18$ and for an applied $V_{sd} = 0.022$ V. The Fermi level, E_F, is taken to be at -5.5 eV. The temperature is so low that the width of the Fermi window is primarily due to V_{sd}. Applying a positive gate voltage will move down in energy the states of the array so that they are within the Fermi window (Figure 9B). Current will increase since the

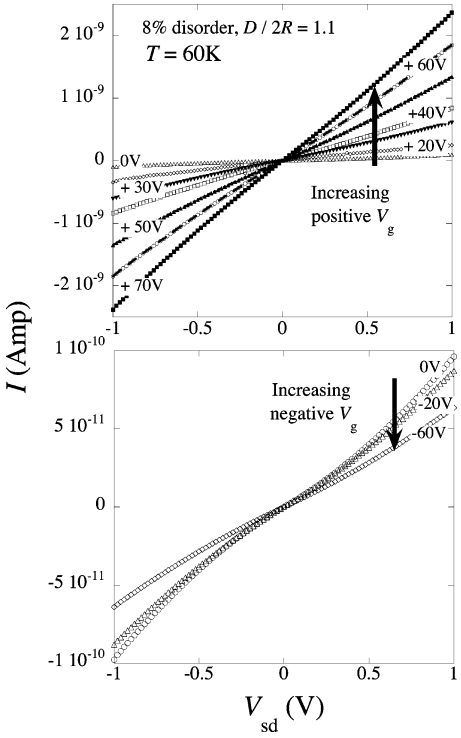

Figure 10. Experimental $I-V$ curves measured for a positive gate voltage (upper panel) and a negative gate voltage (lower panel, note change in the scale of the current). The experimental conditions are as stated on the figure and the gate configuration is shown in Figure 2.

lower lying states have a higher transmission function. Applying a negative V_g leads to a decrease of the current because the states of the array that fall within the detection window have a negligible conduction. Note that the explanation proposed in Figure 9 is not the only possible scenario. It depends on the structure of the band of conducting states and on the Fermi energy of the electrodes. Figure 9 shows why dc conductivity measurements can provide spectroscopic information. V_g can be used to systematically bring the different electronic states of the band within the Fermi window while the magnitude of V_{sd} controls the amount of averaging of the spectrum.

The experimental curves of voltage gating a QD array are plotted in Figure 10. Applying a positive V_g to the array increases the current (top panel) while when a negative V_g is applied (bottom panel), the current remains unchanged and then decreases. The effect of V_g is in agreement with the scheme discussed for Figure 9. It implies that in the absence of an applied V_g, the Fermi energy of the electrode falls close to the bottom of the band of conducting states. As discussed above (see Figure 3), the relative position in energy of the band of conducting states and of the Fermi level of the electrodes strongly depends (for a given electrode composition) on the level of compression applied to the array and on the dot size, which governs the range of the exchange coupling. We show in Figure 11 the computed current for the same array as in Figure 9. The Fermi level of the electrodes is at -5.5 eV, and increasing (positive-valued) V_g are applied. In agreement with the experimental results of Figure 10, the current increases when larger positive V_g are applied. For negative V_g (not shown), the current decreases and becomes too small to be measured because there are no states with a significant transmission function in the Fermi window (Figure 9C).

V. Concluding Remarks

Resonant conduction requires that an orbital of the array that has nonnegligible weight at the two sides in physical contact

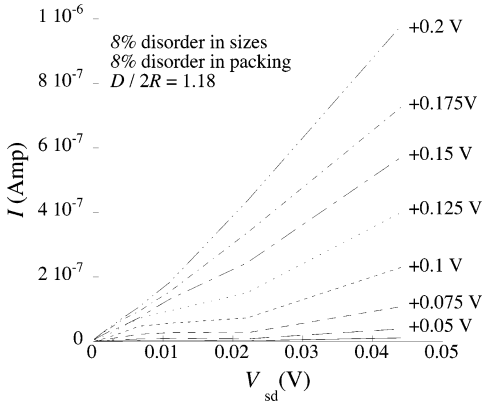

Figure 11. Computed $I-V$ curves for the same array as in Figure 9 and increasing strengths of a positive gate voltage. $T = 200$ K. The current systematically increases when a positive gate voltage is applied because the states at the bottom of the band that have a higher transmission function are brought within the Fermi window. At low bias strengths and applied gate voltage, the current is very low because the Fermi level of the electrodes ($E_F = -5.5$ eV) is located at the bottom of the band (see Figure 9). A negative gate voltage moves the states up in energy so that the current is even smaller, and at some point too small to be measured.

with the electrodes falls in energy within the Fermi window spanned by the electrodes. Otherwise, conduction is by tunneling and is exponentially small. On resonance, the magnitude of the current depends on $|U_L|^2|U_R|^2$ where U_L and U_R are the strength of the coupling between the array and the electrodes. The magnitude of the current depends therefore on a number of material properties. First and foremost is the strength of the exchange coupling between the dots, which transfers the charge across the array. The size of the dots, the variations in size, and the extent of compression of the array control this coupling. In this work we demonstrated the considerable tuning that can be achieved by compression, which allows different orbitals to be in or out of resonance. The Fermi level of the electrodes offers another key variable. Finally, we demonstrated by both experiment and theory that a gate voltage can be used to effectively control the resonance condition. A clear prediction of the theory is that the nature of the gating effect is highly dependent on the degree of compression.

Acknowledgment. The experimental work was supported by the U.S. Department of Energy and a University of California administered CULAR grant. The computational work used facilities provided by NIC (University of Liège) and SFB 377 (Hebrew University of Jerusalem). The work of F.R. is supported by RW.115012 (Région Wallonne) and FRFC 2.4562.03 (FNRS, Belgium). The final stages of this work were supported by the United States−Israel BiNational Science Foundation.

References and Notes

(1) Murray, C. B.; Kagan, C. R.; Bawendi, M. G. *Science* **1995**, *270*, 1335.

(2) Whetten, R. L.; Khoury, J. T.; Alvarez, M. M.; Murthy, S.; Vezmar, I.; Wang, Z. L.; Stephens, P. W.; Cleveland, C. L.; Luedtke, W. D.; Landman, U. *Adv. Mater.* **1996**, *8*, 428.

(3) Ashoori, R. C.; Stormer, H. L.; Weiner, J. S.; Pfeiffer, L. N.; Pearton, S. J.; Baldwin, K. W.; West, K. W. *Phys. Rev. Lett.* **1992**, *68*, 3088.

(4) Collier, C. P.; Mattersteig, G.; Wong, E. W.; Luo, Y.; Beverly, K.; Sampaio, J.; Raymo, F. M.; Stoddart, J. F.; Heath, J. R. *Science* **2000**, *289*, 1172.

(5) Kastner, M. A. *Ann. Phys.* **2000**, *9*, 885.

(6) Davidovic, D.; Tinkham, M. *Phys. Rev. B* **2000**, *61*, R16359.

(7) Beenakker, C. W. J. *Phys. Rev. B* **1991**, *44*, 1646.

(8) Collier, C. P.; Vossmeyer, T.; Heath, J. R. *Annu. Rev. Phys. Chem.* **1998**, *49*, 371.

(9) Murray, C. B.; Kagan, C. R.; Bawendi, M. G. *Annu. Rev. Mater. Sci.* **2000**, *30*.

(10) Schmid, G.; Baumle, M.; Geerkens, M.; Helm, I.; Osemann, C.; Sawitowski, T. *Chem. Soc. Rev.* **1999**, *28*, 179.

(11) Klimov, V. I.; Mikhailovsky, A. A.; Xu, S.; Malko, A.; Hollingsworth, J. A.; Leatherdale, C. A.; Eisler, H. J.; Bawendi, M. G. *Science* **2000**, *290*, 314.

(12) Remacle, F.; Levine, R. D. *ChemPhysChem.* **2001**, *2*, 20.

(13) Beverly, K. C.; Sample, J. L.; Sampaio, J. F.; Remacle, F.; Heath, J. R.; Levine, R. D. *Proc. Natl. Acad. Sci. U.S.A.* **2002**, *99*, 6456.

(14) Black, C. T.; Murray, C. B.; Sandstrom, R. L.; Sun, S. H. *Science* **2000**, *290*, 1131.

(15) Andres, R. P.; Bein, T.; Dorogi, M.; Feng, S.; Henderson, J. I.; Kubiak, C. P.; Mahoney, W.; Osifchin, R. G.; Reifenberger, R. *Science* **1996**, *272*, 1323.

(16) Lin, X. M.; Jaeger, H. M.; Sorensen, C. M.; Klabunde, K. J. *J. Phys. Chem. B* **2001**, *105*, 3353.

(17) Remacle, F.; Levine, R. D. *J. Am. Chem. Soc.* **2000**, *122*, 4084.

(18) Mott, N. F. *Metal−Insulator Transitions*; Taylor & Francis: London, 1990.

(19) Remacle, F.; Levine, R. D. *Proc. Natl. Acad. Sci. U.S.A.* **2000**, *97*, 553.

(20) Collier, C. P.; Saykally, R. J.; Shiang, J. J.; Henrichs, S. E.; Heath, J. R. *Science* **1997**, *277*, 1978.

(21) Beverly, K. C.; Sampaio, J. F.; Heath, J. R. *J. Phys. Chem. B* **2002**, *106*, 2131.

(22) Sampaio, J. F.; Beverly, K. C.; Heath, J. R. *J. Phys. Chem. B* **2001**, *105*, 8797.

(23) Sample, J. L.; Beverly, K. C.; Chaudhari, P. R.; Remacle, F.; Heath, J. R.; Levine, R. D. *Adv. Mater.* **2002**, *114*, 124.

(24) In view of our results on the temperature dependence of the conductivity,[37] there is an obvious interest to extend these measurements to low temperatures.

(25) Remacle, F.; Levine, R. D. *Nano Lett.* **2002**, *2*, 697.

(26) Gallagher, T. F. *Rydberg Atoms*; Cambridge University Press: Cambridge, 1994.

(27) Remacle, F.; Levine, R. D.; Schlag, E. W.; Selzle, H. L.; Held, A. *J. Phys. Chem.* **1996**, *100*, 15320.

(28) This number is not a universal constant. The transition voltage depends on both the size of the array, the compression the degree of disorder, and the temperature. The number we quote is for the arrays of interest here, at low temperatures. See also ref 38.

(29) Levine, R. D. *Quantum Mechanics of Molecular Rate Processes*; Dover: New York, 1999.

(30) Laundauer, R. *IBM J. Res. Dev.* **1957**, *1*, 223.

(31) Imry, Y.; Landauer, R. *Rev. Mod. Phys.* **1999**, *71*, S306.

(32) Imry, Y. *Introduction to Mesoscopic Physics*; Oxford University Press: Oxford, 2002.

(33) Mujica, V.; Kemp, M.; Ratner, M. A. *J. Chem. Phys.* **1994**, *101*, 6849.

(34) Datta, S. *Electronic Transport in Mesoscopic Systems*; Cambridge University Press: Cambridge, 1995.

(35) Nitzan, A. *Annu. Rev. Phys. Chem.* **2001**, *52*, 681.

(36) Remacle, F.; Levine, R. D. *Isr. J. Chem.* **2003**, *42*, 269.

(37) Remacle, F.; Beverly, K. C.; Heath, J. R.; Levine, R. D. *J. Phys. Chem. B* **2002**, *106*, 4116.

(38) Remacle, F.; Levine, R. D. *Appl. Phys. Lett.* **2003**, *82*, 4543.

(39) Remacle, F.; Collier, C. P.; Heath, J. R.; Levine, R. D. *Chem. Phys. Lett.* **1998**, *291*, 453.

(40) Remacle, F.; Collier, C. P.; Markovitch, G.; Heath, J. R.; Banin, U.; Levine, R. D. *J. Phys. Chem. B* **1998**, *102*, 7727.

(41) It is traditional to regard the Stark shift as small unless the field is quite high. The voltages we deal with are small, but so is the array and hence the spacing between the electrodes. In atomic units the electric field strength is 5.14×10^9 V cm^{-1} or 1 V nm^{-1} = 1.95×10^{-3} au. For our case of 0.1 V over 10^4 nm, the field strength is of the order of 2×10^{-8} au.

(42) In principle, the states of the electrodes form a continuum. The coupling of a discrete state to a continuum must be handled with care.[29] This refinement is not essential here because the states of the array form themselves a quasicontinuum. It is essential for more discrete devices, and a study comparing experiment and theory for such systems is in preparation for publication.

(43) Remacle, F.; Levine, R. D. *J. Phys. Chem. A* **2000**, *104*, 10435.

(44) Zallen, R. *The Physics of Amorphous Solids*; Wiley: New York, 1983.

(45) McConnell, H. M. *J. Chem. Phys.* **1961**, *35*, 508.

(46) Shklovskii, B. I.; Efros, A. L. *Electronic Properties of Doped Semiconductors*; Springer-Verlag: Berlin, 1984.